IEEE Access
Multidisciplinary | Rapid Review | Open Access Journal

Received May 17, 2020, accepted May 25, 2020, date of publication June 1, 2020, date of current version June 12, 2020.

Digital Object Identifier 10.1109/ACCESS.2020.2999034

Novel Voltage Balancing Control Strategy for Dual-Active-Bridge Input-Series-Output-Parallel DC-DC Converters

CHENGWEI LUO AND SHOUDAO HUANG, (Senior Member, IEEE)
College of Electrical and Information Engineering, Hunan University, Changsha 410082, China

Corresponding author: Shoudao Huang (hsd1962@ hnu.edu.cn)

This work was supported in part by the National Natural Science Foundation of China under Grant 51737004.

ABSTRACT This paper proposes a novel input voltage balancing control strategy for dual-active-bridge (DAB) input-series-output-parallel (ISOP) DC-DC converters. The proposed strategy not only aims at balancing the input voltage among modules but also at eliminating the coupling effect between input voltage sharing regulators (IVSR) and output voltage regulators (OVR). Specifically, this paper reveals it is too complicated to design a decoupling control structure that can eliminate the dynamic interference of IVSRs to OVRs by using traditional control strategies. Thus, an intermediate control variable, which was adjusted by the IVSR and OVR to simplify the decoupling control structure design, was introduced to calculate the phase-shift ratio. Furthermore, a new control law was derived, and an expression for the intermediate control variable modification was proposed to achieve decoupling control. Moreover, to complete the discussion, the main transfer functions were deduced and the design procedure was illustrated. Based on the novel control strategy, the interference of an IVSR to an OVR was eliminated, so the two controllers can be independently designed. Finally, both the simulation and experimental results were used to verify the performance of the novel control strategy.

INDEX TERMS Dual-active-bridge (DAB) input-series-output-parallel (ISOP) DC-DC converter, decoupling control, dynamic interference, intermediate control variable.

I. INTRODUCTION

High-voltage DC transmission systems are extensively used in rail transit systems, electric vehicle charging systems, and DC grids [1]–[4]. In such applications, the DC supply voltage can reach up to several kilovolts, so it is difficult to directly switch it using a single power semiconductor. Modular input-series-output-parallel (ISOP) DC-DC converters can reduce the voltage level, thus enabling low power-rating switch devices to be used in high input voltage applications. In addition, in comparison with other modular ISOP DC-DC converter structures, the dual-active-bridge (DAB) ISOP DC-DC converter is more suitable for high power applications, as the DAB module has a higher voltage conversion efficiency, and it makes it easy to achieve soft switch and fault isolation [5]–[7]. This paper mainly focuses on DAB ISOP DC-DC converters.

The main objective of the DAB ISOP DC-DC converter control strategy is guaranteeing the transmission power balance among modules since the over-voltage, over-current, and circulating current issues reduce the reliability and power transmission efficiency [8]. The simplest power balancing control strategy is to regulate the transmission power of all the modules by using an output voltage regulator (OVR) [9], [10]. However, due to the inevitable mismatch of the parameters between modules, the transmission power balance cannot only be achieved by the OVR. Many control strategies of ISOP DC-DC converters, including decentralized control strategies and master-slave control strategies, can be used to achieve the transmission power balance of DAB ISOP DC-DC converters. Decentralized control strategies, such as input voltage droop control [11], [12] and output current inverse droop control [13], which are based on the positive

The associate editor coordinating the review of this manuscript and approving it for publication was Chandan Kumar.

output voltage gradient, have the advantages of no control interconnections between modules and simple structures. However, these control strategies have many limitations and poor dynamic and steady-state characteristics [14], [15].

Master-slave control strategies can obtain better characteristics by adding specific sharing regulators, such as output current sharing regulators (OCSR) and input voltage sharing regulators (IVSR), on the basis of the OVR. An OCSR with a cross-feedback control structure exchanges the duty ratio between modules to improve the system stability [16], [17]. In addition, an OCSR with an output current differential control structure uses the output current of an individual module as the rated value for other modules to improve the system reliability [18]. The proposed IVSR in [19] reduces the overshoot of the output voltage in the dynamic response by adding input current control loops. An IVSR with a peak-current control structure uses the sum of the compensation results of the input and output voltages as the rated value for programmed currents to reduce the output voltage disturbance when the DC supply voltage changes significantly [20]. An IVSR with a model predictive control structure improves the system dynamic response by replacing traditional controllers with digital controllers [21]. These master-slave control strategies can not only effectively balance transmission power, but they can also improve the dynamic and steady-state characteristics. However, the coupling effect between OVRs and additional regulators are not analyzed in detail.

The first IVSR with a cross-decoupling control structure was proposed in [22], and it was designed in a small-signal model of a phase-shifted full-bridge (PS-FB) ISOP DC-DC converter. In [23], the small-signal model of a DAB ISOP DC-DC converter was set up, and an IVSR with the same decoupling control structure as that in [22] was proposed. However, in the small-signal model of the ISOP DC-DC converter, the unbalanced input voltage was not considered, as the second-order nonlinear terms were neglected. This can be understood by assuming that the ISOP DC-DC converter operated in a steady-state after the dynamic regulation, which means that the input voltage of the module was converged to a balance [24]. Therefore, the decoupling control structure that was designed in the small-signal model of the system can only eliminate the coupling effect between the controllers in the steady-state operation, but it cannot eliminate the dynamic interference of the IVSR to the OVR when the input voltage of the module is disturbed.

In this paper, the average model of a DAB ISOP DC-DC converter was used to analyze the coupling effect between an IVSR and an OVR. It was revealed that for traditional control strategies, the decoupling control is too hard to achieve in the average model of the system since both controllers directly adjust the phase-shift ratio of the module. Then, a novel input voltage balancing control strategy for the DAB ISOP DC-DC converter was proposed to eliminate the coupling effect between controllers in both steady-state and dynamic operation. By introducing the intermediate control variable, the two controllers could indirectly adjust the phase-shift ratio

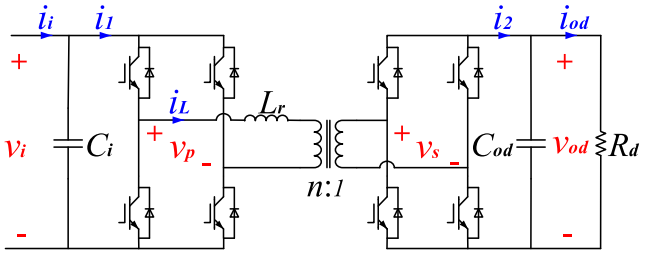

FIGURE 1. Topology of the DAB module.

of the module. This facilitates the design of the decoupling control structure in the average model of the system. Thus, the control circuit of the DAB ISOP DC-DC converter can be decoupled to several independent systems.

This paper is organized as follows: the average model and traditional input voltage balancing control strategy of DAB ISOP DC-DC converter is described in Section II. The theoretical analysis of the novel input voltage balancing control strategy is presented in section III. The design procedure of the OVR and IVSR loops is demonstrated in section IV. In section V, by using a prototype of an ISOP DC-DC converter consist of three DAB modules for simulation and experimental, the novel control strategy is verified to be feasible and effective. Finally, conclusions are drawn in Section VI.

II. AVERAGE MODEL AND TRADITIONAL CONTROL STRATEGY OF DAB ISOP DC-DC CONVERTERS

A. AVERAGE MODEL

The topology of the DAB module, which consists of an isolation transformer and two H-bridges, is shown in Fig. 1. v_i and v_{od} are the input and output voltages of the DAB module, respectively; v_p and v_s are the primary and secondary voltages of the isolation transformer, respectively; i_i and i_{od} are the input and output currents of the DAB module, respectively; i_1 is the input current of the input H-bridge; i_L is the leakage inductance current of the isolation transformer; i_2 is the output current of the output H-bridge; C_i and C_{od} are the input and output DC capacitors of the DAB module, respectively; L_r and n are the leakage inductance and the turns ratio of the isolation transformer, respectively, and R_d is the equivalent load resistance.

To simplify the analysis and calculation, the stray parameters were neglected in this paper. According to [1], the transmission power of the DAB module can be expressed as

$$P = \frac{nd(1-d)v_i v_{od}}{2f_s L_r}, \tag{1}$$

where d is the phase-shift ratio between v_p and v_s, and f_s is the switching frequency. v_p and v_s are square waves with a duty ratio of 50%, and the value of d that is between them is $\pm 1/2$. In another aspect, assuming that the system efficiency is 100%, according to the law of conservation of energy, the transmission power of the DAB module can be

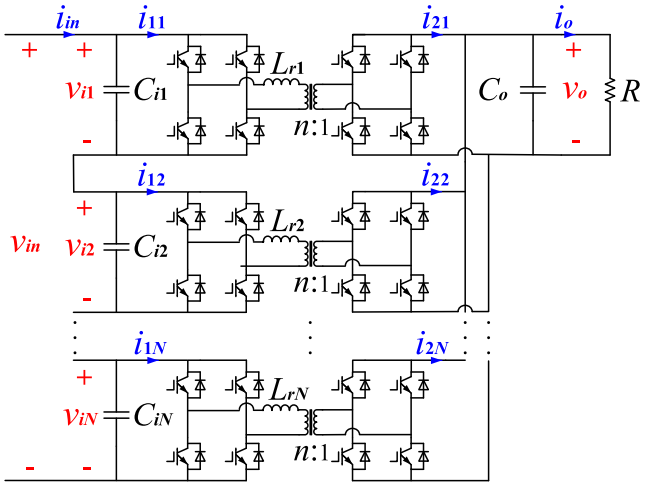

FIGURE 2. Topology of the DAB ISOP DC-DC converter.

expressed as

$$P = v_i i_1 = v_{od} i_2. \tag{2}$$

Then, the average model of the single DAB module can be expressed as

$$\begin{cases} i_1 = \dfrac{nd(1-d)v_{od}}{2f_s L_r} \\ i_2 = \dfrac{nd(1-d)v_i}{2f_s L_r} \end{cases} \tag{3}$$

$$C_i \frac{dv_i}{dt} = i_i - i_1 \tag{4}$$

$$C_{od} \frac{dv_{od}}{dt} = i_2 - \frac{v_{od}}{R_d}. \tag{5}$$

The topology of the ISOP DC-DC converter, which is composed of N DAB modules, is shown in Fig. 2. v_{in} and v_o are the input and output voltages of the ISOP DC-DC converter, respectively; i_{in} and i_o are the input and output currents of the ISOP DC-DC converter, respectively; R and C_o are the equivalent load resistance and output DC capacitor of the ISOP DC-DC converter, respectively; v_{ij} and C_{ij} are the input voltage and input DC capacitor of the j-th DAB module, respectively; i_{1j} is the input current of the input H-bridge of the j-th DAB module; i_{2j} is the output current of the output H-bridge of the j-th DAB module, and L_{rj} is the leakage inductance of the j-th DAB module.

According to (3)-(5), the average model of the DAB ISOP DC-DC converter can be expressed as

$$\begin{cases} i_{1j} = \dfrac{nD_j(1-D_j)}{2f_s L_{rj}} v_o \\ i_{2j} = \dfrac{nD_j(1-D_j)}{2f_s L_{rj}} v_{ij} \end{cases} \tag{6}$$

$$C_{ij} \frac{dv_{ij}}{dt} = i_{in} - i_{1j} \tag{7}$$

$$C_o \frac{dv_o}{dt} = \sum_{j=1}^{N} i_{2j} - \frac{v_o}{R}, \tag{8}$$

where D_j is the phase-shift ratio of the j-th DAB module.

B. TRADITIONAL CONTROL STRATEGY

In the proposed traditional control strategy in [23], the IVSR and the OVR directly adjust the phase-shift ratio of the module through the phase-shift ratio modification and common phase-shift ratio. Therefore, D_j can be expressed as

$$D_j = D_{sj} + D, \tag{9}$$

where D_{sj} is the phase-shift ratio modification of the j-th DAB module, and D is the common phase-shift ratio. Moreover, the decoupling control structure that was designed in the small-signal model of the system can be expressed as

$$D_{sN} = \sum_{j=1}^{N-1} D_{sj}. \tag{10}$$

Supposing that the device parameters of each module are the same. When the input voltage of the system is balanced, (8) can be rewritten as

$$C_o \frac{dv_o}{dt} = \sum_{j=1}^{N} \frac{nD(1-D)}{2f_s L_r} v_{ave} - \frac{v_o}{R}. \tag{11}$$

Among it,

$$v_{ave} = \frac{\sum_{j=1}^{N} v_{ij}}{N}, \tag{12}$$

where v_{ave} is the average input voltage of the DAB module. When the input voltage of the system becomes imbalanced, (8) can be rewritten as

$$\begin{aligned} C_o \frac{dv_o}{dt} &= \sum_{j=1}^{N} \frac{n(D+D_{sj})(1-D-D_{sj})}{2f_s L_r}(v_{ave} - \Delta v_{ij}) - \frac{v_o}{R} \\ &= \sum_{j=1}^{N} \frac{nD(1-D)}{2f_s L_r} v_{ave} - \frac{v_o}{R} + A \end{aligned} \tag{13}$$

Among it,

$$A = \frac{n}{2f_s L_r} \sum_{j=1}^{N} [D_{sj}(1-2D)(v_{ave} - \Delta v_{ij}) - D_{sj}^2 (v_{ave} - \Delta v_{ij})],$$

where Δv_{ij} is the input voltage disturbance of the j-th DAB module.

By comparing (11) and (13), it can be seen that A is the additional term added by the IVSR. The decoupling control structure for the traditional control strategy should eliminate A so that the IVSR does not affect the OVR. To eliminate A, (14) should be satisfied

$$\sum_{j=1}^{N} [D_{sj}(1-2D)(v_{ave} - \Delta v_{ij}) - D_{sj}^2 (v_{ave} - \Delta v_{ij})] = 0. \tag{14}$$

It is clear that the decoupling control structure that was designed in the small-signal model of the system can only satisfy (14) when the input voltage of the system is balanced (steady-state operation condition). In addition, it can be seen

from (14) that the nonlinear terms, which were caused by both the IVSR and OVR directly adjusting the phase-shift ratio of the modules, make the design of the decoupling control structure in the average model of the system too complex. Thus, it is hard to eliminate the dynamic interference of the IVSR to the OVR in the traditional control strategy.

III. NOVEL CONTROL STRATEGY

A. THEORETICAL ANALYSIS

This paper proposes a novel input voltage balancing control strategy by introducing the intermediate control variable so that the interference of the IVSR to the OVR can be easily eliminated.

T_j denotes the intermediate control variable of the j-th DAB module. Since the power in the high-voltage DC transmission system normally flows from the power supply to the load, only the case of $D_j > 0$ was considered.

The relationship between T_j and D_j was defined as

$$\begin{cases} T_j = D_j(1 - D_j) \quad (0 \le T_j \le 1/4) \\ D_j = f(T_j) = \dfrac{1}{2} - \sqrt{\dfrac{1}{4} - T_j}. \end{cases} \tag{15}$$

In the novel control strategy, the intermediate control variable is adjusted by the IVSR and the OVR through intermediate control variable modification and the common intermediate control variable. Therefore, T_j can be expressed as

$$T_j = T_{sj} + T, \tag{16}$$

where T_{sj} is the intermediate control variable modification of the j-th DAB module, and T is the common intermediate control variable.

Supposing that the device parameters of each module are the same, (8) can be rewritten as

$$C_o \frac{dv_o}{dt} = \sum_{j=1}^{N} \frac{nT_j v_{ij}}{2f_s L_r} - \frac{v_o}{R}. \tag{17}$$

When the input voltage of the system is balanced, (17) can be rewritten as

$$C_o \frac{dv_o}{dt} = \sum_{j=1}^{N} \frac{nT}{2f_s L_r} v_{ave} - \frac{v_o}{R}. \tag{18}$$

When the input voltage of the system becomes imbalanced, (17) can be rewritten as

$$\begin{aligned} C_o \frac{dv_o}{dt} &= \sum_{j=1}^{N} \frac{n(T + T_{sj})}{2f_s L_r}(v_{ave} - \Delta v_{ij}) - \frac{v_o}{R} \\ &= \sum_{j=1}^{N} \frac{nT}{2f_s L_r} v_{ave} - \frac{v_o}{R} + B. \end{aligned} \tag{19}$$

Among it,

$$B = \frac{n}{2f_s L_r} \sum_{j=1}^{N} T_{sj}(v_{ave} - \Delta v_{ij}).$$

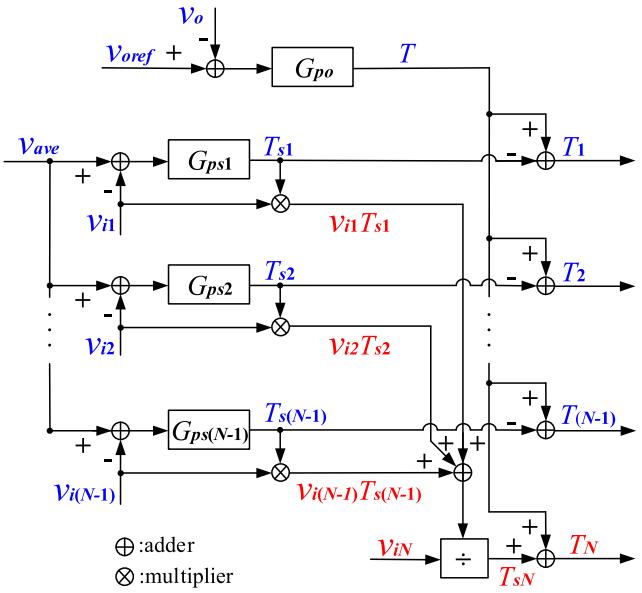

FIGURE 3. Control block diagram of the novel input voltage balancing control strategy.

By comparing (18) and (19), it is clear that B is the additional term added by the IVSR, which is only contains linear components. To eliminate B, (20) should be satisfied

$$\sum_{j=1}^{N} T_{sj}(v_{ave} - \Delta v_{ij}) = 0. \tag{20}$$

Equation (20) describes the relationship among the intermediate control variable modifications. To achieve decoupling control, the intermediate control variable modification of one DAB module should be adjusted by open-loop regulation. Without the loss of generality, in the IVSR, the intermediate control variable modification for the first $N-1$ DAB modules is generated by the PI regulator so as to eliminate the difference between the feedback and the reference values of the input voltage

$$T_{sj} = k_{pj}(v_{ave} - v_{ij}) + k_{ij}(v_{ave} - v_{ij}). \tag{21}$$

Then, the open-loop regulation of the intermediate control variable modification in the Nth DAB module should meet

$$T_{sN} = -\frac{\sum_{j=1}^{N-1} T_{sj}(v_{ave} - \Delta v_{ij})}{v_{iN}} = -\frac{\sum_{j=1}^{N-1} T_{sj} v_{ij}}{v_{iN}}. \tag{22}$$

The control block diagram of the novel control strategy is shown in Fig. 3, where G_{psj} $(j = 1, \ldots, N-1)$ indicates the PI regulators for the first $N-1$ DAB modules in the IVSR, G_{po} indicates the PI regulators in the OVR, v_{oref} is the reference value of the output voltage, and T_{SN} is obtained from (22).

B. SMALL-SIGNAL MODEL

Supposing that the device parameters of each module are the same, when the DAB ISOP DC-DC converter adopts the

novel control strategy, (6) can be rewritten as

$$\begin{cases} i_{1j} = \dfrac{nT_j}{2f_sL_r}v_o \\ i_{2j} = \dfrac{nT_j}{2f_sL_r}v_{ij}. \end{cases} \tag{23}$$

The system was assumed to be operating at a certain steady-state point, where the power supply voltage and the input current are V_{in} and I_{in}, respectively; the output voltage and the average input voltage are V_o and V_{ave}, respectively; the intermediate control variable of the j-th DAB module is T_{jd}, and the input and the output currents of the H-bridge of the j-th DAB module are I_{1j} and I_{2j}, respectively. When the disturbance is applied at this steady-state operation point, the average variables can be rewritten as

$$\begin{cases} i_{1j} = I_{1j} + \tilde{i}_{1j} \\ i_{2j} = I_{2j} + \tilde{i}_{2j} \\ i_{in} = I_{in} + \tilde{i}_{in} \end{cases} \text{ and } \begin{cases} v_o = V_o + \tilde{v}_o \\ v_{ij} = V_{ave} + \tilde{v}_{ij} \\ v_{ave} = V_{ave} + \tilde{v}_{ave} \\ T_j = T_{jd} + \tilde{T}_j. \end{cases}$$

Then, by substituting the above variables into (7), (8), (12), and (23) and by neglecting the steady and the second-order nonlinear terms, we have

$$\begin{cases} \tilde{i}_{1j} = H_{pd}\tilde{T}_j + H_{pv}\tilde{v}_o \\ \tilde{i}_{2j} = H_{sd}\tilde{T}_j + H_{pv}\tilde{v}_{ij} \end{cases} \tag{24}$$

$$\begin{cases} \tilde{v}_{ij} = Z_{in}(\tilde{i}_{in} - \tilde{i}_{1j}) \\ \tilde{v}_o = Z_{out}\sum_{j=1}^{N}\tilde{i}_{2j} \end{cases} \tag{25}$$

$$\tilde{v}_{ave} = \frac{\sum_{j=1}^{N}\tilde{v}_{ij}}{N}. \tag{26}$$

Among them,

$$H_{pd} = \frac{n}{2f_sL_r}V_o, \quad H_{pv} = \frac{n}{2f_sL_r}T_{jd}, \quad H_{sd} = \frac{n}{2f_sL_r}V_{ave}$$
$$Z_{in} = \frac{1}{sC_i}, \quad Z_{out} = \frac{R}{sC_oR+1}.$$

C. MAIN TRANSFER FUNCTIONS

From (24) and (25), $\tilde{v}_{ij}$ was eliminated. Then

$$\tilde{v}_o = \frac{Z_{out}(H_{sd} - Z_{in}H_{pd}H_{pv})\sum_{j=1}^{N}\tilde{T}_j + NZ_{in}Z_{out}H_{pv}\tilde{i}_{in}}{1 + NZ_{in}Z_{out}H_{pv}^2}. \tag{27}$$

Thus, the control-to-output transfer function of the j-th DAB module is

$$G_{vo}(s) = \frac{\tilde{v}_o}{\tilde{T}_j}\bigg|_{\substack{\tilde{i}_{in}=0 \\ \tilde{T}_k=0(k\neq j)}} = \frac{NZ_{out}(H_{sd} - Z_{in}H_{pd}H_{pv})}{1 + NZ_{in}Z_{out}H_{pv}^2}. \tag{28}$$

From (24) and (25), $\tilde{v}_o$ was eliminated. Then

$$\begin{aligned}(1 + Z_{in}Z_{out}H_{pv}^2)\tilde{v}_{ij} + Z_{in}Z_{out}H_{pv}^2\sum_{\substack{k=1 \\ k\neq j}}^{N}\tilde{v}_{ik} \\ = Z_{in}\tilde{i}_{in} - Z_{in}(H_{pd} + Z_{out}H_{sd}H_{pv})\tilde{T}_j \\ - Z_{in}Z_{out}H_{sd}H_{pv}\sum_{\substack{k=1 \\ k\neq j}}^{N}T_k.\end{aligned} \tag{29}$$

Thus, the control-to-input transfer function of the j-th DAB module is

$$G_{vs}(s) = \frac{\tilde{v}_{ij}}{\tilde{T}_j}\bigg|_{\substack{\tilde{v}_{ik}=0 \\ \tilde{T}_k=0(k\neq j)}} = -\frac{Z_{in}(H_{pd} + Z_{out}H_{sd}H_{pv})}{1 + Z_{in}Z_{out}H_{pv}^2}. \tag{30}$$

From (29), we have

$$\begin{aligned}Z_{in}\tilde{i}_{in} = \left(\frac{1 + NZ_{in}Z_{out}H_{pv}^2}{N}\right)\sum_{j=1}^{N}\tilde{v}_{ij} \\ + \left(\frac{Z_{in}H_{pd} + NZ_{in}Z_{out}H_{sd}H_{pv}}{N}\right)\sum_{j=1}^{N}\tilde{T}_j.\end{aligned} \tag{31}$$

By substituting (31) into (29), the average-input-to-module-input transfer function is

$$G_{vsgj}(s) = \frac{\tilde{v}_{ij}}{\tilde{v}_{ave}}\bigg|_{\tilde{T}_j=0} = 1. \tag{32}$$

From (24) and (25), then

$$\tilde{v}_o = Z_{out}H_{sd}\sum_{j=1}^{N}\tilde{T}_j + NZ_{out}H_{pv}\tilde{v}_{ave}. \tag{33}$$

Thus, the average-input-to-output transfer function is

$$G_{vg}(s) = \frac{\tilde{v}_o}{\tilde{v}_{ave}}\bigg|_{\tilde{T}_j=0} = NZ_{out}H_{pv}. \tag{34}$$

D. DECOUPLING THE CONTROL LOOPS

According to Fig. 3, the difference between the feedback and the reference value of the input voltage can be expressed as

$$\tilde{v}_{ij\_er} = \tilde{v}_{ij} - \tilde{v}_{ave}. \tag{35}$$

By neglecting the steady and the second-order nonlinear terms, (16) can be written as

$$\tilde{T}_j = \tilde{T}_{sj} + \tilde{T}. \tag{36}$$

From (28), (30), (35), and (36), we have

$$\begin{bmatrix} \tilde{v}_{i1\_er} \\ \tilde{v}_{i2\_er} \\ \vdots \\ \tilde{v}_{i(N-1)\_er} \\ \tilde{v}_o \end{bmatrix} = H(s)\begin{bmatrix} \tilde{T}_1 \\ \tilde{T}_2 \\ \vdots \\ \tilde{T}_{(N-1)} \\ \tilde{T}_N \end{bmatrix} = H(s)\begin{bmatrix} \tilde{T}_{s1}+\tilde{T} \\ \tilde{T}_{s2}+\tilde{T} \\ \vdots \\ \tilde{T}_{s(N-1)}+\tilde{T} \\ \tilde{T}_{sN}+\tilde{T} \end{bmatrix}. \tag{37}$$

Among it, the $H(s)$ is shown at the bottom of this page. The matrix $H(s)$ can be converted to the product of the two matrices, in which one of them is diagonal matrix. Then, the (37) can be written as

$$\begin{bmatrix} \tilde{v}_{i1\_er} \\ \tilde{v}_{i2\_er} \\ \vdots \\ \tilde{v}_{i(N-1)\_er} \\ \tilde{v}_o \end{bmatrix} = D(s) \begin{bmatrix} \tilde{T}_{s1} \\ \tilde{T}_{s2} \\ \vdots \\ \tilde{T}_{s(N-1)} \\ \tilde{T} \end{bmatrix} - D(s) \sum_{j=1}^{N} \tilde{T}_{sj} \begin{bmatrix} 1/N \\ 1/N \\ \vdots \\ 1/N \\ -1/N \end{bmatrix}. \tag{38}$$

By neglecting the steady and the second-order nonlinear terms, (22) can be written as

$$\tilde{T}_{sN} = \sum_{j=1}^{N-1} \tilde{T}_{sj}. \tag{39}$$

By substituting (39) into (38), we have

$$\begin{bmatrix} \tilde{v}_{i1\_er} \\ \tilde{v}_{i2\_er} \\ \vdots \\ \tilde{v}_{i(N-1)\_er} \\ \tilde{v}_o \end{bmatrix} = D(s) \begin{bmatrix} \tilde{T}_{s1} \\ \tilde{T}_{s2} \\ \vdots \\ \tilde{T}_{s(N-1)} \\ \tilde{T} \end{bmatrix}. \tag{40}$$

According to (40), the simplified control block diagram in Fig. 4 can be obtained, where K_{vc} and K_{vo} are the input and output voltage sensor gains, respectively. Fig. 4 shows that the input voltage sharing loops are decoupled from the output voltage control loop and that they are also decoupled from each other. Thus, by using the novel control strategy, the IVSR loops and the OVR loop can be independently designed.

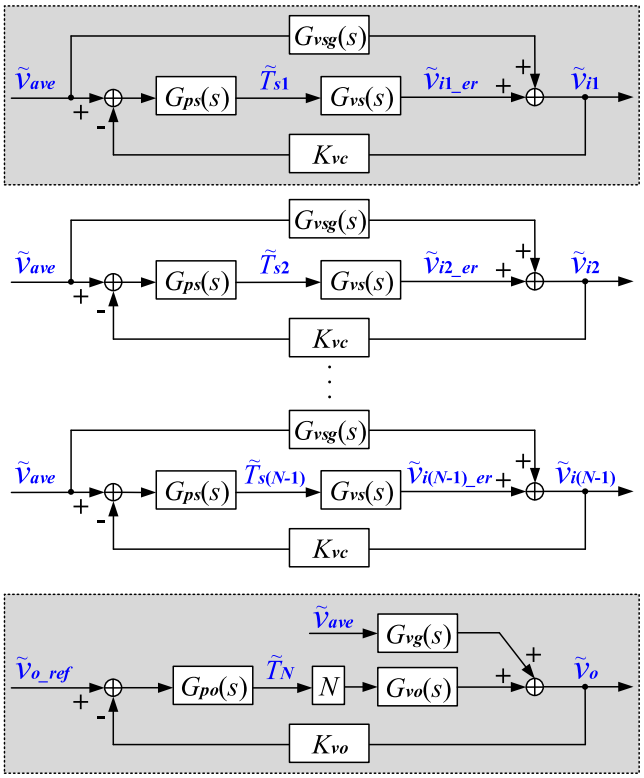

FIGURE 4. Simplified control block diagram of DAB ISOP DC-DC converter.

IV. REGULATOR LOOP DESIGN

An ISOP DC-DC converter consisting of three DAB converters was taken as an example to illustrate the design procedure of the OVR loop and the IVSR loops. The shaded blocks in Fig. 4 represent the output voltage control and the input voltage sharing loops, where $N = 3$.

The specifications of the DAB ISOP DC-DC converter are as follows. The power supply voltage v_{in} is 1200 V, the output voltage v_o is 400 V, and the output DC capacitor C_o is 8 mF. For each DAB module, the input DC capacitor C_{ij} is 4.8 mF, the turn ratio is 1:1, and the leakage inductance L_{rj} is 50 μH. The switching frequency f_s is 50 kHz, and the equivalent load resistance R is 10 Ω. The voltage sensor gains K_{vc} and K_{vo} are 0.005 and 0.09, respectively. The device parameters listed in this paper are obtained by calculation that based on our project requirements and the average model of the DAB ISOP DC-DC converter. For different project, the parameters maybe different from those in this paper but the design procedure of the OVR loop and the IVSR loops are the same.

A. OVR LOOP DESIGN

From Fig. 4, it can be deduced that the gain of the OVR loop is

$$T_{vo}(s) = 3K_{vo}G_{po}(s)G_{vo}(s). \tag{41}$$

The Bode diagrams of the uncompensated OVR loop gain $T_{vo\_u}(s)$ and the compensated loop gain $T_{vo\_c}(s)$ are shown in Fig. 5. As shown in the figure, the uncompensated OVR

$$H(s) = \begin{bmatrix} \frac{G_{vs}(s)(N-1)}{N} & \frac{-G_{vs}(s)}{N} & \cdots & \frac{-G_{vs}(s)}{N} & \frac{-G_{vs}(s)}{N} \\ \frac{-G_{vs}(s)}{N} & \frac{G_{vs}(s)(N-1)}{N} & \cdots & \frac{-G_{vs}(s)}{N} & \frac{-G_{vs}(s)}{N} \\ \vdots & \vdots & \vdots & \vdots & \vdots \\ \frac{-G_{vs}(s)}{N} & \frac{-G_{vs}(s)}{N} & \cdots & \frac{G_{vs}(s)(N-1)}{N} & \frac{-G_{vs}(s)}{N} \\ G_{vd}(s) & G_{vd}(s) & \cdots & G_{vd}(s) & G_{vd}(s) \end{bmatrix}.$$

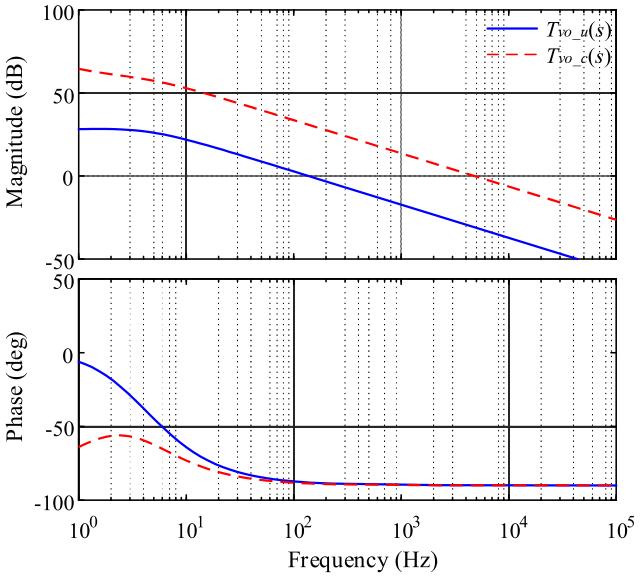

FIGURE 5. Uncompensated and compensated OVR loop gains.

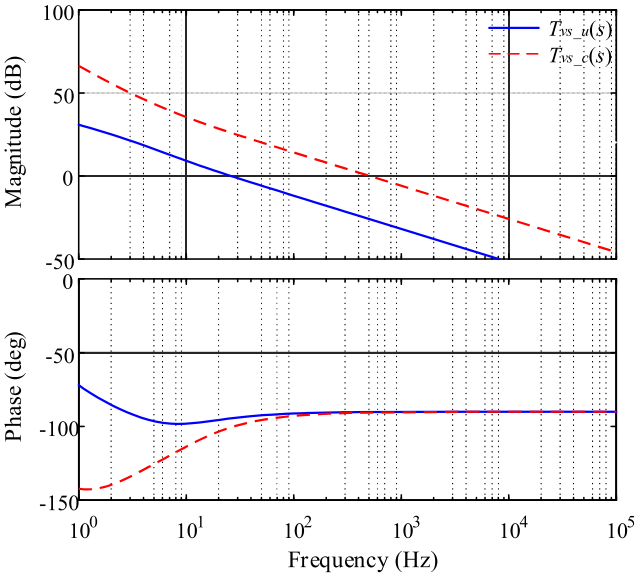

FIGURE 6. Uncompensated and compensated IVSR loop gains.

loop gain is 27 dB at low frequencies, where the crossover frequency is 140 Hz. It was assumed that the target crossover frequency is one-twentieth of the secondary ripple frequency of the switching frequency, which is 5 kHz. In Fig. 5, the uncompensated OVR loop gain, which has a magnitude of 5 kHz, is -31 dB, so the compensator should have a 5 kHz gain of 31 dB.

As presented earlier, a PI controller is used to compensate the OVR loop, and its gain function is as follows:

$$G_{po}(s) = \frac{35s + 500}{s}. \tag{42}$$

In Fig. 5, it can be seen that the compensated OVR loop gain has a crossover frequency of 5 kHz with a phase margin of 85°.

B. IVSR LOOP DESIGN

From Fig. 4, it can be deduced that the gain of the IVSR loop is

$$T_{vs}(s) = K_{vs}G_{ps}(s)G_{vs}(s). \tag{43}$$

The Bode diagrams of the uncompensated IVSR loop gain $T_{vs\_u}(s)$ and the compensated loop gain $T_{vs\_c}(s)$ are shown in Fig. 6. It can be seen that the uncompensated IVSR loop gain is 30 dB at low frequencies and that the crossover frequency is 28 Hz. Since the ripple frequency of the three-phase input rectifier voltage is 300 Hz, the target crossover frequency was chosen to be 500 Hz. In Fig. 6, the uncompensated IVSR loop gain, which has a magnitude of 500 Hz, is -25 dB, so the compensator should have a 500 Hz gain of 25 dB.

The gain function of the PI controller used to compensate the IVSR loop is

$$G_{ps}(s) = \frac{20s + 300}{s}. \tag{44}$$

In Fig. 6, it can be seen that the compensated IVSR loop gain has a crossover frequency of 500 Hz with a phase margin of 90°.

V. SIMULATION AND EXPERIMENTAL RESULTS

A. SIMULATION RESULTS

To verify the effectiveness of the novel control strategy, the MATLAB/Simulink software was used to establish a three-module DAB ISOP DC-DC converter simulation platform according to Fig. 2. The leakage inductances of the three modules are 50 μH, 49 μH, and 51 μH, respectively, and the other parameters are the same as those in section IV. To simulate the input voltage disturbance of the module, resistances of 15 Ω and 30 Ω were connected in parallel with the input capacitors of the first DAB module at 0.15 s and 0.17 s respectively, where the duration was 1 ms. In addition, to clearly show the performance of the decoupling control of the control strategies, the coupling indices M_1 and M_2 were used to represent the absolute values of A under traditional control strategy and B under novel control strategy, respectively. To be more specific, the smaller the value of the coupling index, the better the decoupling control performance of the control strategy.

Fig. 7 shows the values of the coupling indices M_1 and M_2 during the module input voltage disturbance. As shown in Fig. 7, before the module input voltage disturbance, both M_1 and M_2 were approximately equal to zero, meaning that both the control strategies could eliminate the coupling effect between the controllers in the steady-state operation. Unlike M_2, which was still equal to zero during the module input voltage disturbance, M_1 increased during the imbalance and decreased when the module input voltage became balanced again. In addition, the increase in the value of M_1 at 1.5 s was significantly greater than its increase at 1.7 s. Clearly, in the proposed traditional control strategy in [23],

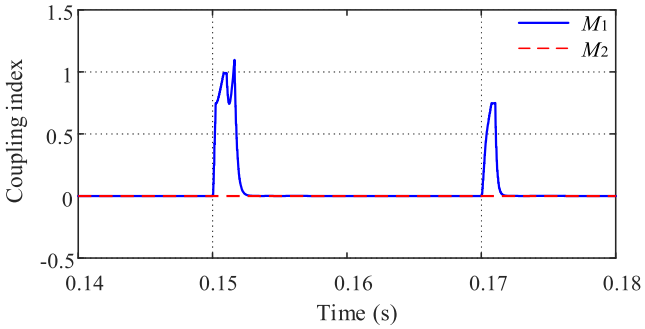

FIGURE 7. The value of the coupling index for the traditional and novel control strategies during the module input voltage disturbance.

the IVSR interferes with the OVR during the module input voltage imbalance (dynamic operation condition). In addition, the wider range of module input voltage imbalance, the larger the interference of the IVSR to OVR. On the contrary, in the novel control strategy, the interference of the IVSR to the OVR was eliminated during both the steady-state and the dynamic operation so that the two controllers can be separately designed for a certain purpose.

B. EXPERIMENTAL RESULTS

To further verify the performance of the novel control strategy, a test was carried out on the three-module DAB ISOP DC-DC converter, where the experimental platform is based on TI TMS320F 28335 DSP. The experimental parameters are as follows. The power supply voltage is 1.2 kV, the output voltage is 400 V, and the load power is 16 kW. The input voltage of each module is 400 V, the turns ratio of the transformer is 1:1, and the other parameters are the same as those in simulation. Due to the open-loop modification manner, the modification mechanism of the input voltage of the third DAB module is different from that of the first and second DAB modules, the DC capacitors of the first and third modules was respectively connected in parallel with a resistance of 15 Ω, where the duration was 1 ms.

Figs. 8 and 9 show the experimental waveforms of the module input voltage and the converter output voltage that were obtained by adopting the traditional and novel control strategies, respectively. From Figs. 8 and 9, it can be seen that under both control strategies, the module input voltage balance could be achieved before and after the module input voltage disturbance. However, under the traditional control strategy, the converter output voltage obviously fluctuated when the module input voltage was disturbed, while under the novel control strategy, the disturbance of the module input voltage did not affect the converter output voltage. Thus, from Figs. 8 and 9, it can be concluded that both the control strategies can achieve an equal performance in balancing the module input voltage when the module parameter is mismatched and after the disturbance. However, unlike the traditional control strategy, the novel control strategy can eliminate the interference of the IVSR to the OVR in dynamic operation.

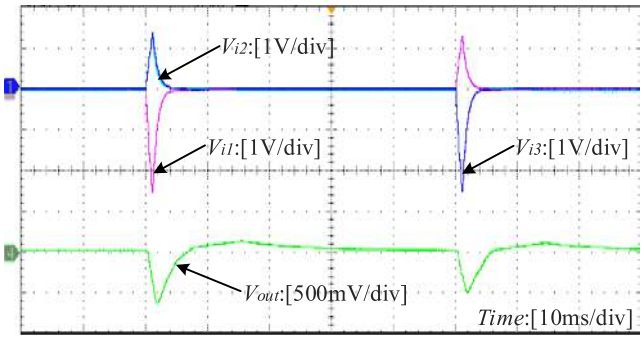

FIGURE 8. Experimental waveforms of the module input voltage and the converter output voltage under the traditional control strategy during the first and third module input voltage disturbance.

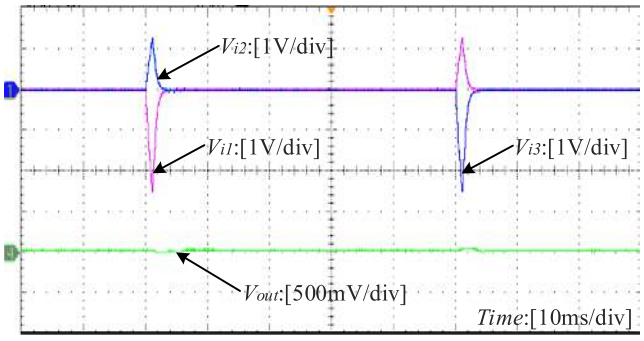

FIGURE 9. Experimental waveforms of the module input voltage and the converter output voltage under the novel control strategy during the first and third module input voltage disturbance.

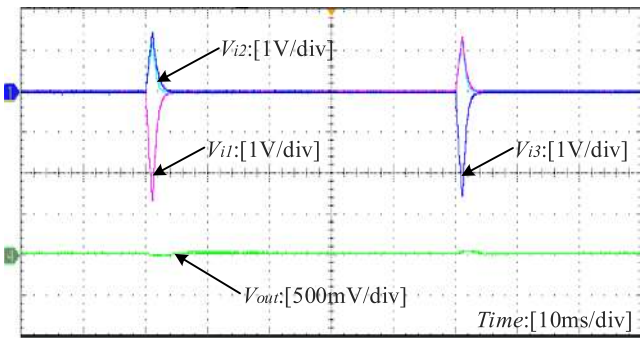

FIGURE 10. Experimental waveforms of the module input voltage and the converter output voltage when the novel control strategy adopts the same OVR control parameters but a different IVSR control parameters.

In the case that the other experimental parameter settings were unchanged, the control parameter settings of the IVSR and the OVR in the novel control strategy were separately adjusted. Fig. 10 shows the experimental waveforms of the module input voltage and the converter output voltage when the novel control strategy adopts the same OVR control parameters but different IVSR control parameters. As shown in Fig. 10, due to the different IVSR control parameter settings, the module input voltage response slightly differed, while the converter output voltage response remained unchanged. Fig. 11 shows the experimental waveforms of the module input voltage and the converter output voltage when the novel control strategy adopts the same IVSR control

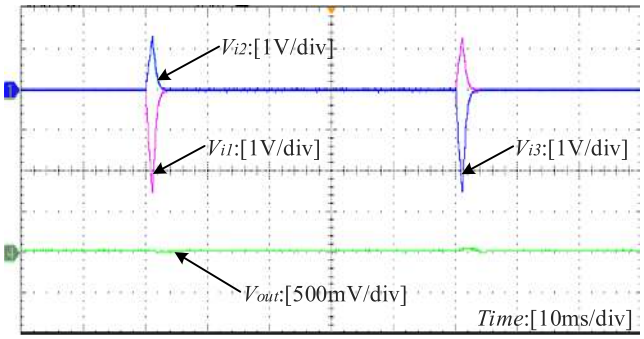

FIGURE 11. Experimental waveforms of the module input voltage and the converter output voltage when the novel control strategy adopts the same IVSR control parameters but a different OVR control parameters.

parameters but different OVR control parameters. As shown in Fig. 11, both the module input voltage and the converter output voltage responses remained unchanged. Thus, the experimental results in Figs. 10 and 11 further confirm that in the novel control strategy, the IVSR is decoupled from the OVR in dynamic operation.

VI. CONCLUSION

The existing decoupling control structure in the traditional input voltage balancing control strategy of DAB ISOP DC-DC converters does not comprehensively consider the coupling effect between the IVSR and the OVR. This study analyzed the coupling effect between the controllers in detail in the average model of the system, and it revealed that, in traditional control strategies, the IVSR is nonlinearly coupled with the OVR, which makes the decoupling control too difficult to achieve. Also, this paper proposes a novel input voltage balancing control strategy in which the decoupling control can be easily achieved by introducing an intermediate control variable that makes the IVSR linearly coupled with the OVR. The simulation and the experimental results verified that the novel control strategy is feasible and effective for balancing input voltages and eliminating the coupling effects between controllers in both steady-state and dynamic operation.

It should be noted that the approach of comprehensively analyzes the coupling effect between controllers in average model can also be applied to other master-slave control strategies of modular ISOP DC-DC converter. In addition, other master-slave control strategies of the DAB ISOP DC-DC converters can also make the additional sharing regulator linearly coupled with the OVR by introducing the intermediate control variable.

REFERENCES

[1] J. Liu, J. Yang, J. Zhang, Z. Nan, and Q. Zheng, "Voltage balance control based on dual active bridge DC/DC converters in a power electronic traction transformer," *IEEE Trans. Power Electron.*, vol. 33, no. 2, pp. 1696–1714, Feb. 2018.

[2] W. Chen, X. Jiang, W. Cao, J. Zhao, W. Jiang, and L. Jiang, "A fully modular control strategy for input-series output-parallel (ISOP) inverter system based on positive output-voltage-amplitude gradient," *IEEE Trans. Power Electron.*, vol. 33, no. 4, pp. 2878–2887, Apr. 2018.

[3] T. Cheng and D. D. C. Lu, "Three-port converters with a flexible power flow for integrating PV and energy storage into a DC bus," *J. Power Electron.*, vol. 17, no. 6, pp. 1433–1444, Nov. 2017.

[4] M. A. Bahmani, T. Thiringer, A. Rabiei, and T. Abdulahovic, "Comparative study of a multi-MW high-power density DC transformer with an optimized high-frequency magnetics in all-DC offshore wind farm," *IEEE Trans. Power Del.*, vol. 31, no. 2, pp. 857–866, Apr. 2016.

[5] K. Zhang, Z. Shan, and J. Jatskevich, "Large- and small-signal average-value modeling of dual-active-bridge DC-DC converter considering power losses," *IEEE Trans. Power Electron.*, vol. 32, no. 3, pp. 1964–1974, Mar. 2017.

[6] J. A. Mueller and J. W. Kimball, "An improved generalized average model of DC-DC dual active bridge converters," *IEEE Trans. Power Electron.*, vol. 33, no. 11, pp. 9975–9988, Nov. 2018.

[7] A. Rodriguez, A. Vazquez, D. G. Lamar, M. M. Hernando, and J. Sebastian, "Different purpose design strategies and techniques to improve the performance of a dual active bridge with phase-shift control," *IEEE Trans. Power Electron.*, vol. 30, no. 2, pp. 790–804, Feb. 2015.

[8] W. Chen, X. Ruan, H. Yan, and C. K. Tse, "DC/DC conversion systems consisting of multiple converter modules: Stability, control, and experimental verifications," *IEEE Trans. Power Electron.*, vol. 24, no. 6, pp. 1463–1474, Jun. 2009.

[9] R. Giri, V. Choudhary, R. Ayyanar, and N. Mohan, "Common-duty-ratio control of input-series connected modular DC-DC converters with active input voltage and load-current sharing," *IEEE Trans. Ind. Appl.*, vol. 42, no. 4, pp. 1101–1111, Jul. 2006.

[10] V. Choudhary, E. Ledezma, R. Ayyanar, and R. M. Button, "Fault tolerant circuit topology and control method for input-series and output-parallel modular DC-DC converters," *IEEE Trans. Power Electron.*, vol. 23, no. 1, pp. 402–411, Jan. 2008.

[11] W. Chen and G. Wang, "Decentralized voltage-sharing control strategy for fully modular input-series-output-series system with improved voltage regulation," *IEEE Trans. Ind. Electron.*, vol. 62, no. 5, pp. 2777–2787, May 2015.

[12] W. Chen, G. Wang, X. Ruan, W. Jiang, and W. Gu, "Wireless input-voltage-sharing control strategy for input-series output-parallel (ISOP) system based on positive output-voltage gradient method," *IEEE Trans. Ind. Electron.*, vol. 61, no. 11, pp. 6022–6030, Nov. 2014.

[13] G. Xu, D. Sha, and X. Liao, "Decentralized inverse-droop control for input-series-output-parallel DC-DC converters," *IEEE Trans. Power Electron.*, vol. 30, no. 9, pp. 4621–4625, Sep. 2015.

[14] L. Qu and D. Zhang, "Input voltage sharing control scheme for input series and output series DC/DC converters using paralleled MOSFETs," *IET Power Electron.*, vol. 11, no. 2, pp. 382–390, Feb. 2018.

[15] M. Abrehdari and M. Sarvi, "Comprehensive sharing control strategy for input-series output-parallel connected modular DC-DC converters," *IET Power Electron.*, vol. 12, no. 12, pp. 3105–3117, Oct. 2019.

[16] D. Sha, Z. Guo, and X. Liao, "Cross-feedback output-current-sharing control for input-series-output-parallel modular DC-DC converters," *IEEE Trans. Power Electron.*, vol. 25, no. 11, pp. 2762–2771, Nov. 2010.

[17] D. Sha, K. Deng, and X. Liao, "Duty cycle exchanging control for input-series-output-series connected two PS-FB DC-DC converters," *IEEE Trans. Power Electron.*, vol. 27, no. 3, pp. 1490–1501, Mar. 2012.

[18] L. Qu, D. Zhang, and Z. Bao, "Output current-differential control scheme for input-series-output-parallel-connected modular DC-DC converters," *IEEE Trans. Power Electron.*, vol. 32, no. 7, pp. 5699–5711, Jul. 2017.

[19] P. J. Grbovic, "Master/slave control of input-series- and output-parallel-connected converters: Concept for low-cost high-voltage auxiliary power supplies," *IEEE Trans. Power Electron.*, vol. 24, no. 2, pp. 316–328, Feb. 2009.

[20] L. Qu, D. Zhang, and B. Zhang, "Input voltage sharing control scheme for input series and output parallel connected DC-DC converters based on peak current control," *IEEE Trans. Ind. Electron.*, vol. 66, no. 1, pp. 429–439, Jan. 2019.

[21] Q. Wei, B. Wu, D. Xu, and N. R. Zargari, "Model predictive control of capacitor voltage balancing for cascaded modular DC-DC converters," *IEEE Trans. Power Electron.*, vol. 32, no. 1, pp. 752–761, Jan. 2017.

[22] X. Ruan, W. Chen, L. Cheng, C. K. Tse, H. Yan, and T. Zhang, "Control strategy for input-series-output-parallel converters," *IEEE Trans. Ind. Electron.*, vol. 56, no. 4, pp. 1174–1185, Apr. 2009.

[23] P. Zumel, L. Ortega, A. Lazaro, C. Fernandez, A. Barrado, A. Rodriguez, and M. M. Hernando, "Modular dual-active bridge converter architecture," *IEEE Trans. Ind. Appl.*, vol. 52, no. 3, pp. 2444–2455, May/Jun. 2016.
[24] X. She, A. Q. Huang, T. Zhao, and G. Wang, "Coupling effect reduction of a voltage-balancing controller in single-phase cascaded multilevel converters," *IEEE Trans. Power Electron.*, vol. 27, no. 8, pp. 3530–3543, Aug. 2012.

CHENGWEI LUO was born in Hunan, China, in 1992. He received the B.S. degree in electrical engineering from Baylor University, Waco, TX, USA, in 2013, and the M.S. degree in electrical engineering from The University of Sheffield, Sheffield, U.K., in 2015. He is currently pursuing the Ph.D. degree in electrical engineering with Hunan University, Changsha, Hunan, China. His current research interests include the control of multilevel converters and renewable energy generation.

SHOUDAO HUANG (Senior Member, IEEE) was born in Hunan, China, in 1962. He received the B.S. and Ph.D. degrees in electrical engineering from Hunan University, Changsha, China, in 1983 and 2005, respectively. He is currently a full-time Professor with the College of Electrical and Information Engineering, Hunan University. His current research interests include the motor design and control, poelectronic system and control, and wind energy conversion systems.